



Universiteit Utrecht

FACULTY OF SCIENCE
DEPARTMENT OF PHYSICS AND ASTRONOMY
SUBATOMIC PHYSICS

BACHELOR THESIS

Peak Shapes in TOF PID histograms

Author:
Karindra PERRIER

Supervisors:
Marco van LEEUWEN
Misha VELDHOEN

June 21, 2013

Abstract

In TOF PID histograms the peaks of all non-centered particles are deformed due to subtraction of the wrong expected time. We reproduce the deformed peak shapes, first by means of a Monte Carlo simulation, then by a numerical calculation processed into a Spline function. The results of the different methods are compared and proven to be consistent. A convolution with the detector resolution is performed to incorporate detector effects. The Spline is fitted to data from ALICE. A straight forward fit delivered a $\chi_{red}^2 = 4333$. To improve the fit crude adjustments, only justified within the scope of further research, were made. A better $\chi_{red}^2 = 419$ was found changing the radius of the detector by 10cm. And the best fit with $\chi_{red}^2 = 379$ integrated a scaling factor of which the origin is unknown.

Contents

1	Introduction	3
2	Theory	4
2.1	Derivation of time for TOF detector	4
2.2	Derivation of dN/dT distribution	5
2.3	Convolution	6
3	Constructing the dN/dT Distribution without detector effects	8
3.1	Distribution by means of a Monte Carlo Method	8
3.1.1	Figure 5(g): $5.0 < p_T < 5.1$ GeV/c	8
3.1.2	Figure 5(e): $2.0 < p_T < 2.1$ GeV/c	9
3.1.3	Figure 5(a)&(h): $0.5 < p_T < 0.7$ GeV/c	9
3.1.4	“Corner values”	9
3.2	Distribution by means of a Numerical Calculation	12
4	Constructing the dN/dT Distribution taking detector resolution into account	15
4.1	Convolution of the Monte Carlo Distribution	15
4.2	Convolution of the Numerical Spline Function	16
5	Comparison to ALICE data	18
5.1	Fit to centered peak	18
5.2	Fit to deformed peak with non-uniform momentum distribution	18
5.3	Fit to deformed peak with exponential tail and constant added	20
5.4	Fit to deformed peak with scaling factor	21
6	Conclusion and Outlook	23
7	Acknowledgments	23

1 Introduction

The ALICE detector is designed to detect particles that are produced in collisions, such as Pb-Pb and p - p collisions. It contains several subdetectors that measure different parameters of the incoming particles. An essential part of the ALICE experiment is the Particle IDentification (PID). Sometimes the mass difference of the particles makes it possible to select a range for which the identity can be assumed, but often the particle yields lie within close range to each other and the overlapping peaks make an accurate particle count difficult. A solution to this problem would be to determine the yield by means of a fit to the peak. For a good fit the form of the peak needs to be well understood. Unfortunately these peak shapes often turn out to be a deformation of your standard Gaussian function.

This deformation occurs because of the following. The ALICE data is assembled into histograms where a certain particle is usually set to be the expected particle. The data is then centered for this particular particle by subtracting the expected values. For instance, the Time of Flight (TOF) detector measures the time it takes for a particle to move from the collision to the detector. When TOF expects a particle i , it will subtract the expected time Δt_i from the measured time, presenting a peak around $T = 0$. However, when any other particle comes in the wrong time is subtracted, resulting into a deformed peak around $T \neq 0$. Since the expected time is related to the momentum and pseudorapidity, the deformation is too.

We can better our understanding of the deformation by looking at the TOF measurements in Figure 1. On the horizontal axis we have the transverse momentum, on the vertical axis we have the particle velocity in $\beta = v/c$. Since all particles have different masses we can distinguish separate strips of particle counts with a Gauss-like smear. Centering one of the particles would be like straightening out one of these strips, coincidentally bending the other strips. Since the velocity is related to the time, the peaks are a result of a vertical slice of the histogram being compressed in horizontal direction, eliminating momentum dependence. We thus compress the strips, deforming the Gauss-like smear they had.

For the TOF detector we try to reproduce the deformed peaks as to make a good fit and accurate determination of the yields possible. In the Theory section we derive the necessary equations. After treating the essential equation for the time of flight, we find an expression for the time distribution by performing a coordinate transformation on the momentum- and pseudorapidity distributions. In the mid-sections we use the found relation in a Monte Carlo simulation, constructing the time distribution. The same time distribution is constructed using a different method, building Spline functions by means of a numerical calculation. Since detector effects should be taken into account we convolute the time distributions with the detector resolution in the fourth section. Lastly we compare our results to data from ALICE, using different tactics in several fits. We close with a conclusion and outlook.

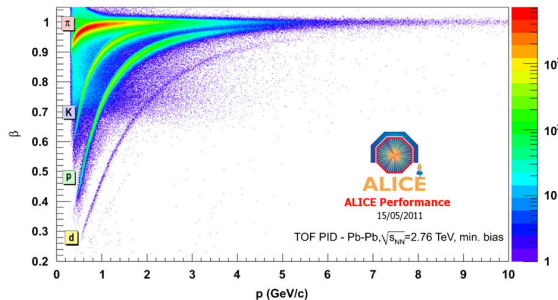


Figure 1: TOF measured particle $\beta = v/c$ vs. transverse momentum for Pb-Pb collisions. [1]

2 Theory

2.1 Derivation of time for TOF detector

The time it takes a particle to travel from the collision to the detector is measured by the Time of Flight detector. TOF is one of the cylindrical detectors around the beam, see Figure 2. In this thesis we will consider pion, kaon and proton hits, so we assume the particle has a charge of $q = \pm e$. When we look at the transverse plane, the magnetic field of $B = 0.5$ parallel to the detector axis will bend the particle track in the shape of a circle (see Fig. 2, right) with radius R :

$$R = \frac{p_T}{eB}, \quad (1)$$

where p_T is the momentum transverse to the magnetic field. Given the length of the particle's arced track L_{arc} , and its velocity transversal to the magnetic field v_T we can express the time it takes for the particle to hit the TOF detector as follows:

$$\Delta t = \frac{L_{\text{arc}}}{v_T} = \frac{\alpha R}{v_T} = \frac{\alpha p_T}{eBv_T}, \quad (2)$$

where $0 < \alpha < \pi$ is the angle that the particle travels along the circle with radius R . This α can be found with simple geometrics as follows:

$$\sin(\alpha/2) = L_{\text{TOF}}/2R = eBL_{\text{TOF}}/2p_T. \quad (3)$$

where L_{TOF} is the radius of the Time of Flight detector.

Note that $0 < eBL_{\text{TOF}}/2p_T < 1$, hence the minimum transverse momentum that a particle needs to reach the TOF detector is: $p_{T,\text{min}} = eBL_{\text{TOF}}/2 \simeq 285\text{MeV}/c^1$.

The time Δt can now be written as:

$$\Delta t = \frac{2p_T}{eBv_T} \arcsin\left(\frac{eBL_{\text{TOF}}}{2p_T}\right) \quad (4)$$

We now express Δt in the transverse momentum p_T and pseudorapidity η , using the relations $\gamma v_T = p_T/m$, $\gamma v_z = p_z/m$, and $p_T^2 \cosh^2 \eta = p_T^2 + p_z^2$.

It is evident that:

$$\gamma^2(1 - v^2/c^2) = 1$$

¹The elementary charge and the values from Table 1 where used.

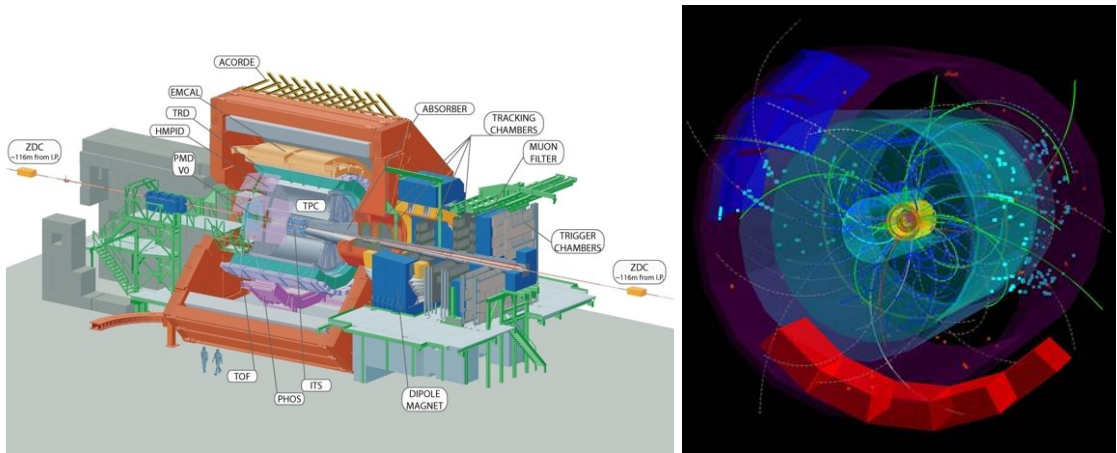


Figure 2: Left: Schematic representation of the ALICE detector. Right: Graphic visualisation of particle tracks [3]

We can rewrite this:

$$\gamma^2 - 1 = \gamma^2 v^2 / c^2 = \gamma^2 (v_T^2 + v_z^2) / c^2 = (p_T^2 + p_z^2) / m^2 c^2 = p_T^2 \cosh^2 \eta / m^2 c^2.$$

Hence:

$$\gamma = \sqrt{1 + \frac{p_T^2}{m^2 c^2} \cosh^2 \eta} = \frac{p_T}{mc} \sqrt{\frac{m^2 c^2}{p_T^2} + \cosh^2 \eta}. \quad (5)$$

Using this, we find:

$$\frac{p_T}{v_T} = m\gamma = \frac{p_T}{c} \sqrt{\frac{m^2 c^2}{p_T^2} + \cosh^2 \eta}. \quad (6)$$

Hence the final result is:

$$\Delta t = \frac{2p_T}{eBc} \arcsin \left(\frac{eBL_{\text{TOF}}}{2p_T} \right) \sqrt{\frac{m^2 c^2}{p_T^2} + \cosh^2 \eta}. \quad (7)$$

2.2 Derivation of dN/dT distribution

The particle yields in a TOF histogram can be determined with a dN/dT_{ij} distribution where T_{ij} expresses the measured time Δt_i of particle i minus the expected time Δt_j of particle j . From Equation (7) we know that:

$$T_{ij}(p_T, \eta) = \frac{2p_T}{eBc} \arcsin \left(\frac{eBL}{2p_T} \right) \left[\sqrt{\frac{m_i^2 c^2}{p_T^2} + \cosh^2 \eta} - \sqrt{\frac{m_j^2 c^2}{p_T^2} + \cosh^2 \eta} \right] \quad (8)$$

The dN/dT_{ij} distribution is the result of a coordinate transformation of the $d^2N/dp_T d\eta$ distribution. There are two equally valid ways to transform the distribution, given the TOF histograms are computed over a p_T range $[p_{Tmin}, p_{Tmax}]$ and an η range $[\eta_{min}, \eta_{max}]$. Either we determine $\eta(T_{ij}, p_T)$, use that $|dT/d\eta|^{-1} = |d\eta/dT|^2$ and integrate over p_T such that:

$$\begin{aligned} \frac{dN}{dT_{ij}}(T_{ij}) &= \int_{p_{Tmin}}^{p_{Tmax}} dp_T \frac{d^2N}{dT_{ij} dp_T} \times B_{\eta_{min}}^{\eta_{max}}(\eta(T_{ij}, p_T)) = \int dp_T \frac{d\eta}{dT_{ij}} \frac{d^2N}{dp_T d\eta} \times B_{\eta_{min}}^{\eta_{max}}(\eta(T_{ij}, p_T)) \\ &= \int dp_T \left| \frac{dT_{ij}}{d\eta} \right|^{-1} (\eta(T_{ij}, p_T), p_T) \times \frac{d^2N_i}{d\eta dp_T}(\eta(T_{ij}, p_T), p_T) \times B_{\eta_{min}}^{\eta_{max}}(\eta(T_{ij}, p_T)) \end{aligned} \quad (9)$$

Where $B_{min}^{max}(x)$ is a Boxcar function³.

Or we determine $p_T(T_{ij}, \eta)$, use that $|dT/dp_T|^{-1} = |dp_T/dT|$ and integrate over η :

$$\begin{aligned} \frac{dN}{dT_{ij}}(T_{ij}) &= \int_{\eta_{min}}^{\eta_{max}} d\eta \frac{d^2N_i}{dT_{ij} d\eta} \times B_{p_{Tmin}}^{p_{Tmax}}(p_T(T_{ij}, \eta)). \\ &= 2 \int_0^{\eta_{max}} d\eta \left| \frac{dT_{ij}}{dp_T} \right|^{-1} (p_T(T_{ij}, \eta), \eta) \times \frac{d^2N_i}{dp_T d\eta}(p_T(T_{ij}, \eta), \eta) \times B_{p_{Tmin}}^{p_{Tmax}}(p_T(T_{ij}, \eta)). \end{aligned} \quad (10)$$

We will continue our derivation with the latter.

It is reasonable to assume that that the $dN/d\eta$ distribution is uniform, so we take $d^2N/dp_T d\eta$ to be independent of η . However, the dN/dp_T distribution is not uniform. We know that a typical transverse momentum distribution has a peak around the particles mass with an exponentially

²This is allowed because $T_{ij}(p_T)$ is a bijection for fixed η .

³Boxcar $B_{min}^{max}(x) = \Theta(x - min) \times \Theta(max - x)$. Where $\Theta(x)$ is the Heaviside step function.

decreasing tail at higher momenta, see Figure 3. Later on we want to be able to determine the dN/dp_T distribution from the fit. To make a systematic approach of an accurate description of dN/dp_T possible, we assume we can approximate the distribution by developing it as a polynomial series in p_T :

$$\frac{d^2 N_i}{dp_T d\eta} = \sum_n C_n p_T^n, \quad \text{for: } n = 0, 1, 2, \dots, \quad (11)$$

We then define:

$$\left. \frac{dN_i}{dT_{ij}} \right|_{\eta_{min}, p_{Tmin}}^{\eta_{max}, p_{Tmax}} = \sum_n C_n g_n(T_{ij}), \quad (12)$$

where:

$$g_n(T_{ij}) \equiv 2 \int_0^{\eta_{max}} d\eta \left| \frac{dT_{ij}}{dp_T} \right|^{-1} (p_T(T_{ij}, \eta), \eta) \times p_T^n(T_{ij}, \eta) \times B_{p_{Tmin}}^{p_{Tmax}}(p_T(T_{ij}, \eta), \eta). \quad (13)$$

When we assume that the momentum ranges used for the histograms are small enough that we can truncate the series after the first two terms the distribution can be expressed as follows:

$$\frac{dN}{dp_T} = C_0 + C_1 p_T \quad (14)$$

and we can use a simplification of Equation (12):

$$\left. \frac{dN_i}{dT_{ij}} \right|_{\eta_{min}, p_{Tmin}}^{\eta_{max}, p_{Tmax}} = C_0 g_0 + C_1 g_1 \quad (15)$$

2.3 Convolution

The TOF detector has a resolution of approximately 150ps. Therefore the obtained expression for the dN/dT_{ij} distribution needs to be convoluted with a Gaussian distribution in order to describe the experimental data.

$$\left(\frac{dN}{dT} * G \right) (T) = \int_{-\infty}^{\infty} d\tau \frac{dN}{dT}(\tau) G(t - \tau) \quad (16)$$

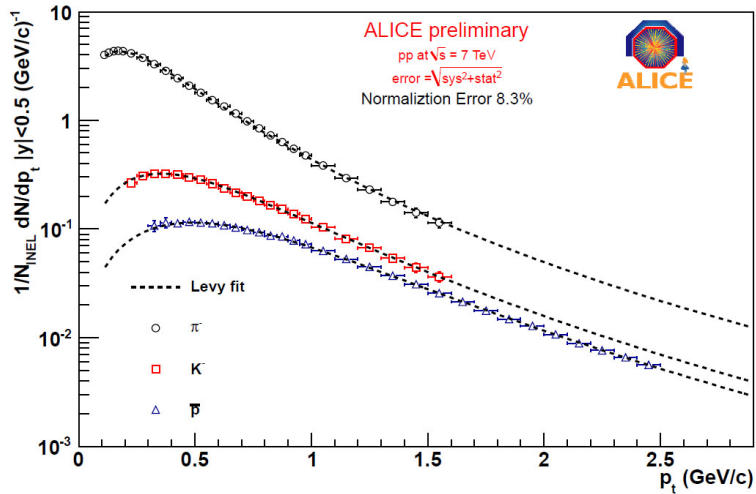


Figure 3: Typical transverse momentum spectra of π , K and p [2]

Note that when the expected time is the same as the measured time, i.e., TOF expected the particle that was measured, we have that $T_{i,i} = 0$ and $dN/dT_{i,i}$ is a Dirac delta function. The convolution of this distribution will return the Gaussian distribution, and we retrieve the uncertainty distribution of the detector, as expected.

3 Constructing the dN/dT Distribution without detector effects

To reproduce the TOF peaks we first need to construct the dN/dT_{ij} distribution expressed in Equation (15). We will first simulate dN/dT_{ij} by use of a Monte Carlo method. After that we will construct dN/dT_{ij} with a different method, building a Spline out of a numerical representation of Equation (15). We will use the standard values for the TOF detector and particle masses displayed in Table 1.

Magn.Fld: $ \vec{B} $	0.5 T
Radius TOF: L_{TOF}	3.8 m
Pion Mass	0.139570 GeV/c
Kaon Mass	0.493667 GeV/c
Proton Mass	0.938272 GeV/c

Table 1: Standard values used for the simulation

Because the momentum of the particle as well as the width of the momentum range affect the shape of the distribution dramatically we will simulate the distribution for several momentum ranges. Also we will investigate different combinations of particle yields related to the time of flight of the expected particle (the centered particle).

TOF has an pseudorapidity range of $-0.8 < \eta < 0.8$, for bigger pseudorapidities the particle won't hit the detector. Therefore the pseudorapidity range for all plots is $|\eta| < 0.8$.

3.1 Distribution by means of a Monte Carlo Method

The most simple way to obtain the expected distribution is by use of a Monte Carlo method. We will start out with both a uniform $dN/d\eta$ and dN/dp_T distribution. From these distributions we draw a random value for $\eta \in [-0.8, 0.8]$ and $p_T \in [p_{Tmin}, p_{Tmax}]$. The random values for η and p_T will give us a value $T_{ij}(p_T, \eta)$ given by Equation (8). The Monte Carlo histograms are typically filled with $\sim 10^5$ entries of T_{ij} generated in this way.

Figure 5 shows the histograms of the dN/dT_{ij} distribution for several momentum ranges, obtained through a Monte Carlo method. The shape of the histograms originate from the $T_{ij}(p_T, \eta)$ function plotted in Figure 4 for kaons with a pion expectation. The dN/dT_{ij} distribution can be seen as a projection of the $T_{ij}(p_T, \eta)$ function, or - to be precise - the section of $T_{ij}(p_T, \eta)$ for which $\eta \in [-0.8, 0.8]$ and $p_T \in [p_{Tmin}, p_{Tmax}]$. First the function is projected onto the (T, p_T) -plane, after which this whole plane is projected onto the T -axis. Or similarly, one can imagine the projection of the T_{ij} function onto the (T, η) -plane, after which the (T, η) -plane is again projected onto the T -axis.

Figure 4 shows a plot of the time $T_{ij}(p_T, \eta)$. We see that for higher momenta there is a smaller time difference between the time of flight of the particles. In other words, at high momenta the mass difference between the particles becomes less important. The pseudorapidity dependence of the function therefore becomes more significant at higher momenta.

3.1.1 Figure 5(g): $5.0 < p_T < 5.1$ GeV/c

Imagine taking a slice from the surface in Figure 4 from $p_T = 5.0$ to $p_T = 5.1$ GeV/c, the slice is indicated in blue in the graph. In this slice T_{ij} is almost independent of p_T and, as mention before, the symmetric curved η dependence becomes dominant (see the separate depiction of the slice to the right in Figure 4). This means that the distribution in the histogram would be determined strongly by the projection of the symmetric η curve. The resulting histogram is shown in Figure 5(g). The cut-offs are almost vertical (an indication of the small deformation by p_T) and in between we recognize the shape of the compressed η curve, which is the positive half of the doubled inverted curve.

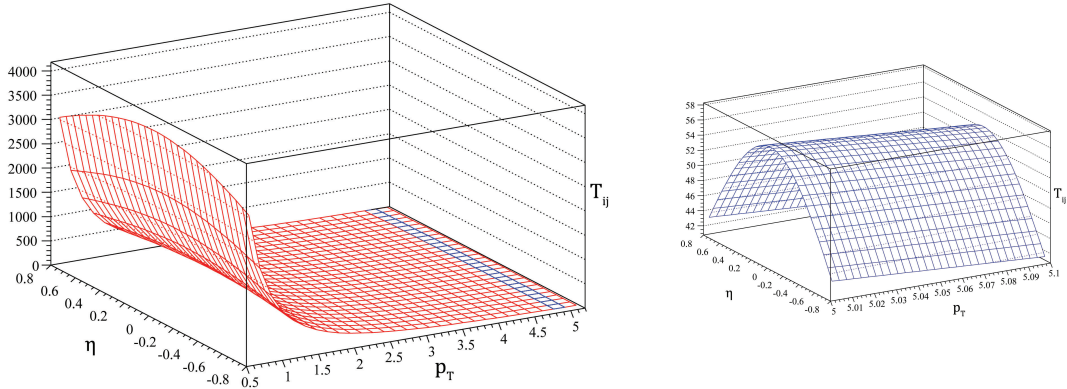


Figure 4: $T_{K,\pi}(p_T, \eta)$ with time in picoseconds and momenta in GeV/c. In blue a slice from $5.0 < p_T < 5.1$ GeV/c that is separately plotted to the right.

3.1.2 Figure 5(e): $2.0 < p_T < 2.1$ GeV/c

This effect is less pronounced but still visible at the momentum range of $2.0 < p_T < 2.1$ depicted in (e) of Figure 5. Since the slope of the T_{ij} function in the p_T direction determines the slope of the cut-offs we have that the cut-offs broaden for smaller momenta.

3.1.3 Figure 5(a)&(h): $0.5 < p_T < 0.7$ GeV/c

This relation between momentum and time difference is also reflected in the fact that for higher p_T ranges the peak is located at smaller $|T_{ij}|$ and becomes narrower, whereas for low p_T the peak is very wide and located at high $|T_{ij}|$ like in (a).

We also see that, as one would expect, $dN/dT_{ij}(T_{ij})$ and $dN/dT_{ji}(T_{ji})$ are each other's image mirrored in the dN/dT -axis, see (h) for a reflection of (a).

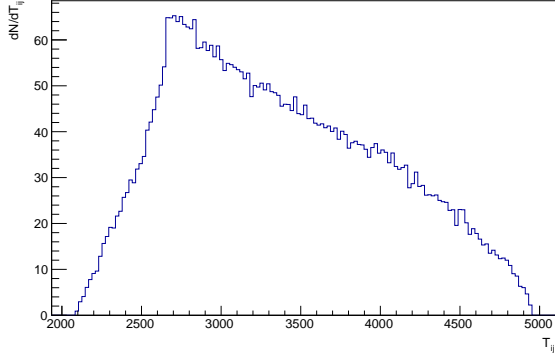
3.1.4 “Corner values”

In (e) and (g) of Figure 5 we can make out four points where the derivative is discontinuous, these distinct “Corners” become more pronounced for higher p_T . Comparing (e) and (f) one can easily see that the left limit of the distribution corresponds to the lowest point in T_{ij} around 240 ps. The left limit of the peak is therefore expressed by $T_{min} = T_{ij}(p_{Tmax}, 0.8)$. In that same way we can deduct that $T_{max} = T_{ij}(p_{Tmin}, 0)$.

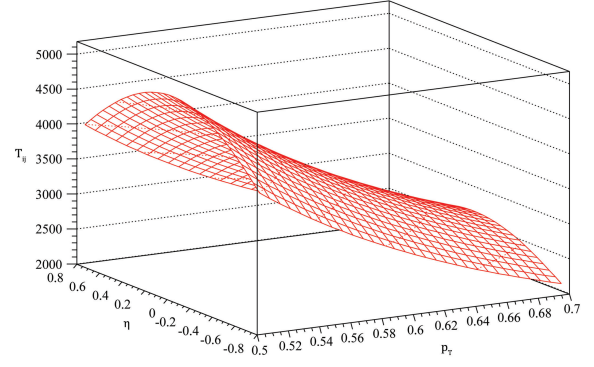
There are two other sharp corners in the $T_{ij}(p_T, \eta)$ graph and both translate to the dN/dT_{ij} distribution in the following way: $T_{\eta\pm} = T_{ij}(p_{Tmin}, 0.8)$ and $T_{\eta0} = T_{ij}(p_{Tmax}, 0)$. When, at low p_T the slope of T_{ij} as a function of p_T becomes bigger, the η dependence of T_{ij} becomes less important and the inside corners are mostly determined by the value of p_T . This is why at low p_T we have that $T_{\eta\pm} = T_{ij}(p_{Tmin}, 0.8) > T_{\eta0} = T_{ij}(p_{Tmax}, 0)$. At high momenta η becomes more important and therefore in these ranges $T_{\eta\pm} = T_{ij}(p_{Tmin}, 0.8) < T_{\eta0} = T_{ij}(p_{Tmax}, 0)$. The fact that $T_{\eta\pm} = T_{ij}(p_{Tmin}, 0.8)$ and $T_{\eta0} = T_{ij}(p_{Tmax}, 0)$ approach each other in value is reflected in (c) of Figure 5, the corners have become indistinguishable from each other.

	T_{min}	$T_{\eta\pm}$	$T_{\eta0}$	T_{max}
$0.5 < p_T < 0.7 \text{ GeV/c}$	2086 ps	3994 ps	2663 ps	4950 ps
$0.7 < p_T < 0.8 \text{ GeV/c}$	1609 ps	2086 ps	2073 ps	2663 ps
$2.0 < p_T < 2.1 \text{ GeV/c}$	240 ps	264 ps	319 ps	351 ps
$5.0 < p_T < 5.1 \text{ GeV/c}$	41 ps	43 ps	55 ps	57 ps

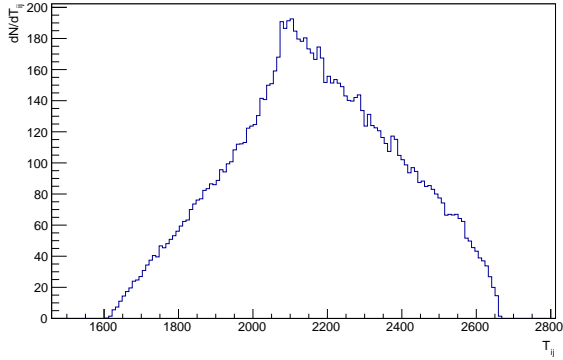
Table 2: Corner values of $T_{K,\pi}(p_T, \eta)$



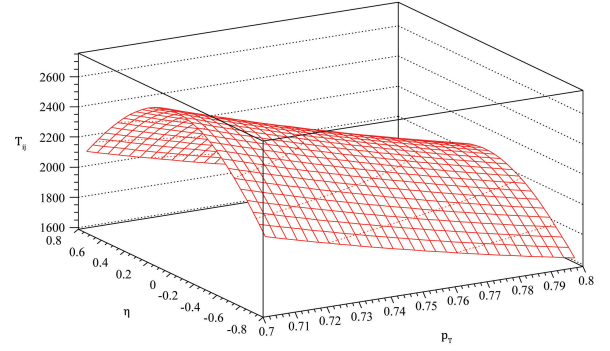
(a) $0.5 < p_T < 0.7$ GeV/c, $i = K, j = \pi$



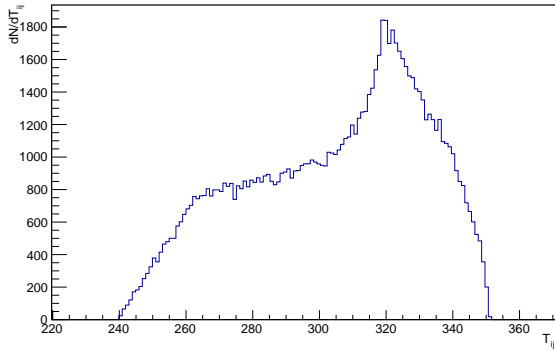
(b) $T_{K,\pi}(p_T, \eta)$ for $0.5 < p_T < 0.7$ GeV/c



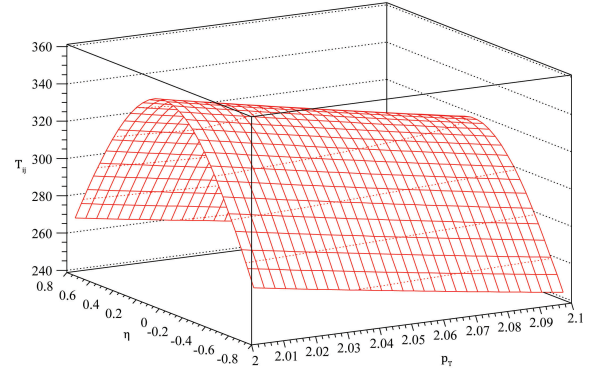
(c) $0.7 < p_T < 0.8$ GeV/c, $i = K, j = \pi$



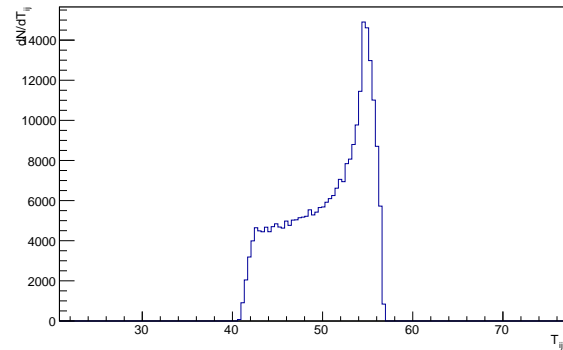
(d) $T_{K,\pi}(p_T, \eta)$ for $0.7 < p_T < 0.8$ GeV/c



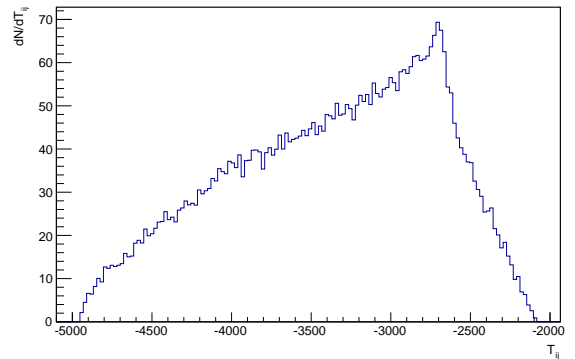
(e) $2.0 < p_T < 2.1$ GeV/c, $i = K, j = \pi$



(f) $T_{K,\pi}(p_T, \eta)$ for $2.0 < p_T < 2.1$ GeV/c



(g) $5.0 < p_T < 5.1$ GeV/c, $i = K, j = \pi$



(h) $0.5 < p_T < 0.7$ GeV/c, $i = \pi, j = K$

Figure 5: Panels a, c, e, g and h: Monte Carlo Simulated Histograms of the dN/dT_{ij} distribution. The time differences of particle i are plotted in relation to the expected time of particle j for different momentum ranges. Time differences are in picoseconds and momenta in GeV/c. All histograms have a uniform momentum distribution of $dN/dp_T = 1$. Panels b, d and f: The segment of T_{ij} that was used to make the histogram left of these panels.

Note that for T_{ij} where the mass of $j > i$, all these values are mirrored in the dN/dT_{ij} -axis and T_{min} becomes T_{max} .

When a particle is centered its expected time is set to zero, this particle will give an narrow peak at $T = 0$ much like a Dirac delta function. Figure 6 illustrates the deformed peak the other particles will give.

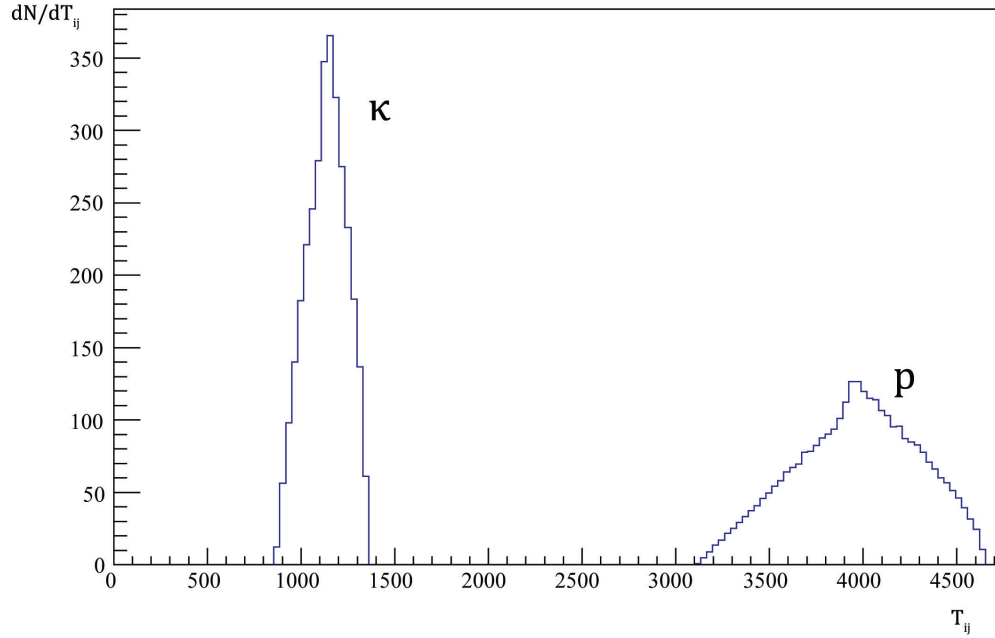


Figure 6: Pion centered histogram for $1.0 < p_T < 1.1$ GeV/c. The kaons and protons experience the simulated deformation. Since the mass difference is biggest for the proton, it will experience the most deformation. The peak of the pion itself is not plotted, it would be a high sharp peak at 0.

3.2 Distribution by means of a Numerical Calculation

The Monte Carlo histograms are insightful but not very practical when we want to make fits to data. Therefore we want a function with parameters that can be used to do a fit. To find dN/dT_{ij} expressed in Equation (15) we need an expression for $p_T(T_{ij}, \eta)$. Unfortunately the T_{ij} function of Equation (8) is not invertible, so we must determine $p_T(T_{ij}, \eta)$ numerically by use of a root finder. We used a Brent's root finding algorithm. When we have the momentum in terms of the time difference and pseudorapidity, we can take the derivative dT_{ij}/dp_T of the time difference to the momentum (analytically) and express it in terms of T_{ij} and η (numerically).

$$\begin{aligned} \frac{dT_{ij}}{dp_T}(p_T(T_{ij}, \eta), \eta) = & \\ & \frac{2p_T(T_{ij}, \eta)}{eBc} \arcsin\left(\frac{eBL}{2p_T(T_{ij}, \eta)}\right) \left[-\frac{c^2m_i^2}{p_T^3(T_{ij}, \eta)\sqrt{\frac{c^2m_i^2}{P_T^2(T_{ij}, \eta)} + \cosh^2(\eta)}} + \frac{c^2m_j^2}{p_T^3(T_{ij}, \eta)\sqrt{\frac{c^2m_j^2}{P_T^2(T_{ij}, \eta)} + \cosh^2(\eta)}} \right] \\ & - \frac{eBL}{p_T(T_{ij}, \eta)eBc\sqrt{1 - \frac{e^2B^2L^2}{4p_T^2(T_{ij}, \eta)}}} \left[\sqrt{\frac{c^2m_i^2}{P_T^2(T_{ij}, \eta)} + \cosh^2(\eta)} - \sqrt{\frac{c^2m_j^2}{P_T^2(T_{ij}, \eta)} + \cosh^2(\eta)} \right] \\ & + \frac{2}{eBc} \arcsin\frac{eBL}{2p_T(T_{ij}, \eta)} \left[\sqrt{\frac{c^2m_i^2}{P_T^2(T_{ij}, \eta)} + \cosh^2(\eta)} - \sqrt{\frac{c^2m_j^2}{P_T^2(T_{ij}, \eta)} + \cosh^2(\eta)} \right] \end{aligned} \quad (17)$$

We now effectively projected the function onto the (T_{ij}, η) -plane, eliminating p_T dependence from the function. Because $T_{ij}(p_T)$ for fixed η is a bijection we can use that $|dT_{ij}/dp_T|^{-1} = |dp_T/dT_{ij}|$ and we can find the values for g_n from Equation (13) leading us to dN/dT_{ij} by numerical integration over η .

Calculations with the numeric function use quite some cpu power, so the numerical values we find for Equation (15) are processed into a Spline. A Spline is a function that is build out of a series of points where the value of the function, as well as several derivatives in that point, are determined. The Spline then draws a line through the points, satisfying the constraints of the derivatives. We will use a Spline that determines four derivatives. The procedure is as follows⁴:

The purpose of the procedures is to determine the interpolating quintic natural Spline function $S(x)$ for the set of data points (x_i, y_i) , $i = N1, N1+1, \dots, N2$, where it is assumed that $x_{N1} < x_{N1+1} < \dots < x_{N2}$. The interpolating quintic natural Spline function $S(x)$ with the knots x_{N1}, \dots, x_{N2} has the following properties:

- (i) $S(x)$ is a polynomial of degree 5 in each interval (x_i, x_{i+1}) , $i = N1, \dots, N2 - 1$.
- (ii) $S(x)$ and its derivatives $S'(x)$, $S''(x)$, and $S'''(x)$ are continuous in $[x_{N1}, x_{N2}]$.
- (iii) $S''(x_{N1}) = S''(x_{N2}) = S'''(x_{N1}) = S'''(x_{N2}) = 0$.
- (iv) $S(x_i) = y_i$, $i = N1, \dots, N2$.

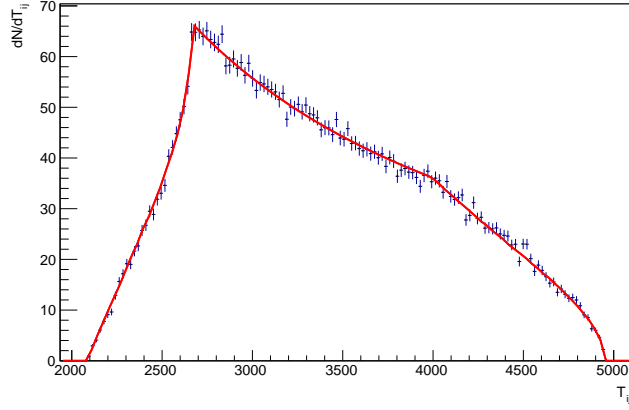
It is known that if $N2 > N1 + 1$, then there is a unique quintic natural Spline function which has the properties (i)-(iv). This Spline function can be represented in the form:

$$S(x) = y_i + B_it + C_it^2 + D_it^3 + E_it^4 + F_it^5 \quad (18)$$

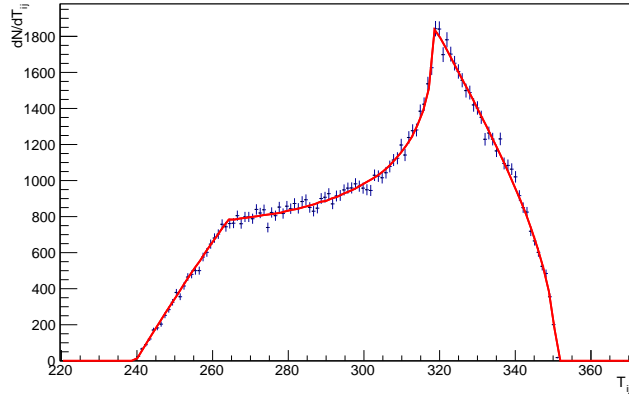
with $t = x - x_i$, for $x_i < x < x_{i+1}$, $i = N1, \dots, N2 - 1$.

⁴Quoted from: ALGORITHM 507 Procedures for Quintic Natural Spline Interpolation [E1], John G. Herriot, Stanford University and Christian H. Reinsch, Leibniz-Rechenzentrum der Bayerischen Akademie der Wissenschaften, Germany

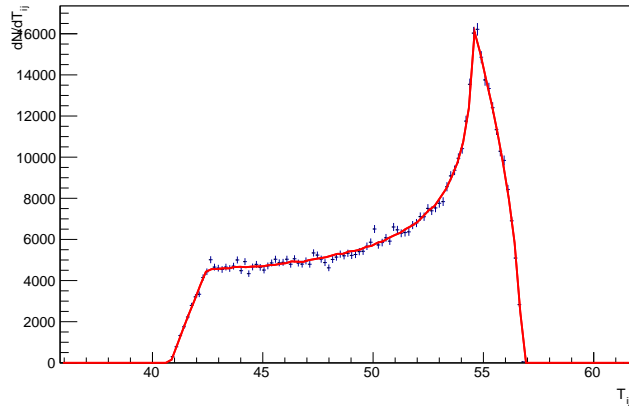
Figure 7 shows a plot of dN/dT_{ij} together with the Monte Carlo histogram for several momentum ranges. The Monte Carlo and Spline function are consistent with each other, which is reflected by the reduced Chi-squared⁵ values of the order of 1 (see Figure 7). Since we retrieved the dN/dT_{ij} distribution in two different ways, the satisfactory fit gives us confidence our methods are processed correctly. However, it does not give us any guaranties regarding the used values from table 1 or the used equations of the Theory section.



(a) $0.5 < p_T < 0.7$ GeV/c, $\chi^2 = 9.38$, $\chi_{red}^2 = 1.07$



(b) $2.0 < p_T < 2.1$ GeV/c, $\chi^2 = 150.6$, $\chi_{red}^2 = 0.88$



(c) $5.0 < p_T < 5.1$ GeV/c, $\chi^2 = 638.1$, $\chi_{red}^2 = 0.91$

Figure 7: Splines of the numerical function fitted tot the Monte Carlo histograms of the dN/dT distribution. For all graphs $i = K$, $j = \pi$. A uniform momentum distribution of $dN/dp_T = 1$ was used.

⁵The χ_{red}^2 values where calculated by dividing the the χ^2 by the number of bins used for the fit.

In the previous section we solely looked at uniform dN/dp_T distributions. In reality we know the momentum distribution not to be uniform. As discussed in the Theory section we will approximate the distribution with the linear function $dN/dp_T = C_0 + C_1 p_T$. We will use our stored Splines to build the resulting distribution. Figure 8 gives us an example of such a linear combination of the g_0 and g_1 Splines. To demonstrate the different possibilities a uniform momentum distribution, a distribution with a positive slope and a distribution with a negative slope are used to make the dN/dT_{ij} distributions.

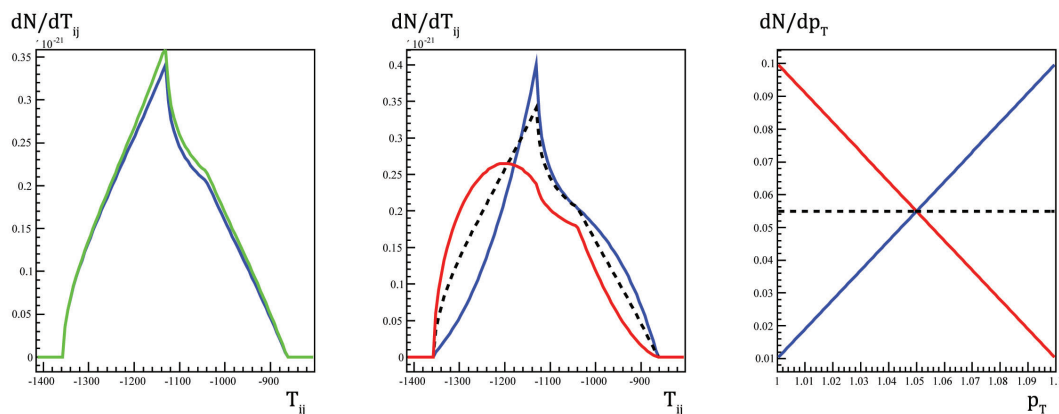


Figure 8: Example of linear combinations of g_0 and g_1 . At the left g_0 (blue) and g_1 (green) are plotted. In the central graph three dN/dT_{ij} functions with different dN/dp_T distributions are plotted: $dN/dp_T = 1 - 0.9p_T$ (red), $dN/dp_T = 0.55$ (black and dashed), $dN/dp_T = -0.89 + 0.9p_T$ (blue). The distributions for dN/dp_T are plotted in the right graph.

4 Constructing the dN/dT Distribution taking detector resolution into account

In the previous section we simulated the dN/dT_{ij} distribution measured by a perfect detector. Of course the TOF detector is not perfect, it has an uncertainty of ~ 150 ps. We simulate the uncertainty of the TOF detector by convoluting the dN/dT_{ij} distribution found in the previous section with a Gaussian distribution.

4.1 Convolution of the Monte Carlo Distribution

The Monte Carlo that generated the dN/dT distribution is easily adjusted to simulate the convolution. After the value of $T_{ij}(p_T, \eta)$ for random values $p_T \in [p_{Tmin}, p_{Tmax}]$ and $\eta \in [-0.8, 0.8]$ is determined, we can make a Gaussian distribution around this value of T_{ij} and draw a random value from this Gaussian distribution. The histogram is then filled with these values for the time T_{ij} . Figure 9 displays the $dN/dT_{\pi,p}$ distribution for $1.0 < p_T < 1.1$ GeV/c, where a Gaussian distribution with a $\sigma = 150$ ps was used.

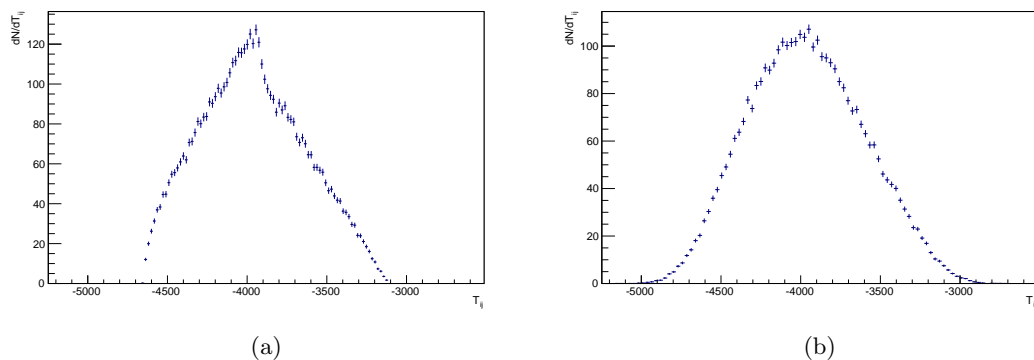


Figure 9: Unconvoluted (a) and convoluted (b) dN/dT_{ij} distributions generated by means of a Monte Carlo method for $1.0 < p_T < 1.1$ GeV/c, $i = \pi$, $j = p$. For the convolution a Gaussian distribution with a $\sigma = 150$ ps was used.

We can see that around these momenta the convoluted distribution shows a big resemblance to a Gaussian distribution. The deformation effect is therefore hardly noticeable. A smaller value for the σ in the Gaussian distribution or a lower momentum range will retrieve a peak that retains more of the characteristic features of the original dN/dT_{ij} distribution. An example of a convolution with a smaller σ of 100 ps is shown in Figure 10.

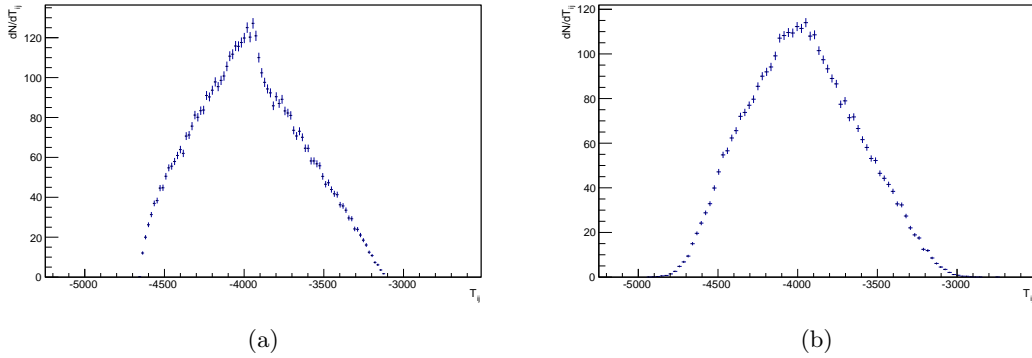


Figure 10: Unconvoluted (a) and convoluted (b) dN/dT_{ij} distributions generated by means of a Monte Carlo method for $1.0 < p_T < 1.1$ GeV/c, $i = \pi$, $j = p$. For the convolution a Gaussian distribution with a $\sigma = 100$ ps was used.

For the convolution in Figure 9 we centered the proton and plotted the pion hits. The mass difference between the particles is the biggest difference possible in this set of particles, thus the deformation too is biggest for this combination of particles. For other combinations we would have to look at even lower momentum ranges than $1.0 < p_T < 1.1$ GeV/c to notice the deformation. A plot of a pion distribution with proton expectation at a lower momentum range of $0.5 < p_T < 0.7$ GeV/c is given in Figure 11. It is clear the characteristics of the deformation are significant even after the convolution.

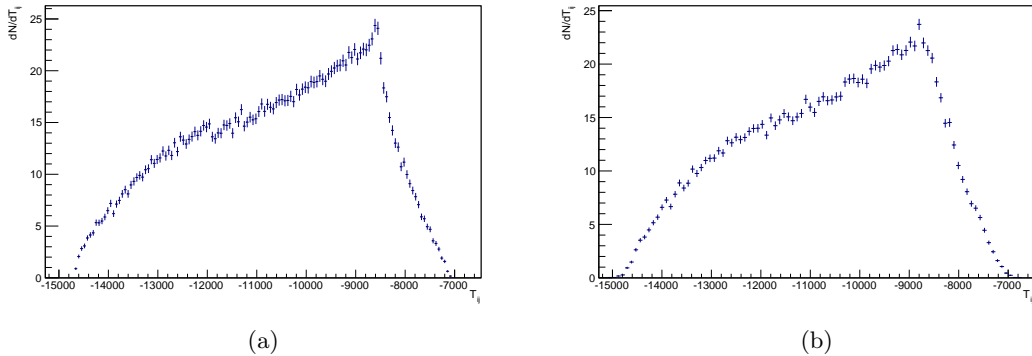
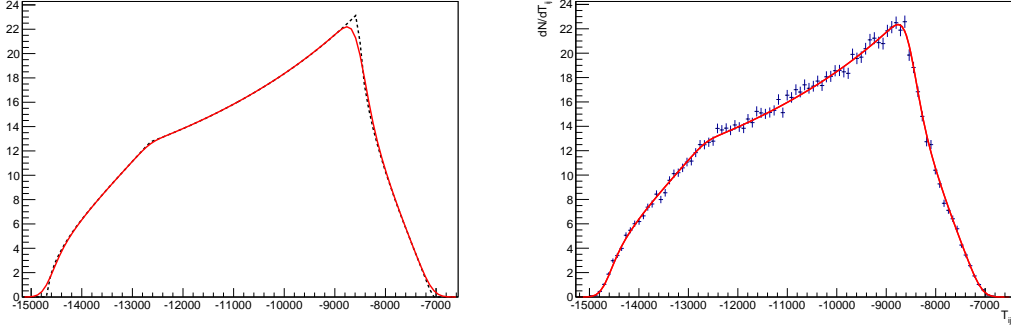


Figure 11: Unconvoluted (a) and convoluted (b) dN/dT_{ij} distributions generated by means of a Monte Carlo method for $0.5 < p_T < 0.7$ GeV/c, $i = \pi$, $j = p$. For the convolution a Gaussian distribution with a $\sigma = 150$ ps was used.

Note that no actual convolution has been performed on the dN/dT_{ij} distributions. The convolution was simulated by drawing random values from a Gaussian distribution as described.

4.2 Convolution of the Numerical Spline Function

For the numerical function we invoke the stored g_n Splines, build our desired dN/dT_{ij} function, and perform a numerical convolution on it. Figure 12(a) shows the function of the original dN/dT_{ij} distribution and the convoluted dN/dT_{ij} distribution. For this convolution we used a uniform dN/dp_T distribution, which comes down to the values $C_0 = 1$ and $C_1 = 0$ in Equation (15).



(a) Convoluted $dN/dT_{\pi,p}$ distribution (red) and (b) Convoluted $dN/dT_{\pi,p}$ distribution generated by original $dN/dT_{\pi,p}$ distribution (black and dashed) the numerical function (red) and Monte Carlo histogram (blue). A fit of the function to the histogram with the normalization factor as a parameter gives a $\chi_{red}^2 = 0.76$

Figure 12: $dN/dT_{\pi,p}$ distributions for $0.5 < p_T < 0.7$ GeV/c, $i = \pi$, $j = p$. For the convolution a Gaussian distribution with a $\sigma = 150$ ps was used.

Figure 12(b) shows this convoluted dN/dT_{ij} distribution fitted to the same distribution generated by the Monte Carlo method. The only parameter for the fit was the normalization factor. The reduced chi-squared value of $\chi_{red}^2 = 0.76$ shows us the two methods are consistent with each other.

5 Comparison to ALICE data

We now have a numerical expression for a convoluted dN/dT_{ij} distribution that should simulate the deformation that particle hits experience when any other particle than the particle at hand is expected. We can verify the simulation against the data in a fit. Figure 13 shows the TOF PID pion and kaon hits for a kaon expectation. Since the time of flight for the kaon is centered the kaon hits render a Gauss-like peak around zero. The pions have a smaller mass and hit the detector earlier than expected, therefore they render a deformed peak in the negative time range. Note a low and broad p_T range was chosen to make the deformation very pronounced.

5.1 Fit to centered peak

Presumably, the kaon hits experience the same uncertainty distribution the pion hits undergo. We thus fit the Gaussian distribution to the centered kaon peak to find the standard deviation σ . Besides σ the only other parameter of the fit is the normalization factor N_K . Subsequently we fit to the deformed pion peak, taking the found value for σ as a fixed parameter and leaving only the normalization factor N_π as a free parameter. Figure 14(a) shows both fits. It is clear that the simulation does not fit the data very well. We have a terrible $\chi^2_{red,\pi}$ of 6.5×10^4 for the fit on the pion peak and an even worse $\chi^2_{red,K}$ of 9.1×10^6 for the fit on the kaon peak.

Before we try to improve our fit we shortly discuss the normalization factors. When the Gauss and Splines are normalized the fit parameters N_K and N_π can be used to determine the particle ratio. This ratio can be compared to the ratio of the data. For the data $N_\pi/N_K = 13.8$ and for the simulation $N_\pi/N_K = 14.9$, which is a difference of 8%.

5.2 Fit to deformed peak with non-uniform momentum distribution

One of the problems in the previous fit lies in the slope of the peak. We can adjust the slope by making the coefficients C_0 and C_1 of Equation (15) parameters of the fit. This makes non-uniform dN/dp_T distributions possible. Since C_0 and C_1 are of no relevance to the centered peak – this peak is merely the product of a Dirac delta function convoluted with the detector resolution – we now fit to the pion peak.

Also, we add the parameter μ to the fit which translates the center of the of the Gauss. And – because we don't want the background noise to effect our fit – we limit our fits to a smaller range, cutting of the end tails of the fit. Figure 14(b) shows the resulting fit to the pion peak. We have a better value for the Chi-squared of $\chi^2_{red} = 4333$. However, when we use the same parameters on the centered kaon peak, keeping only the normalization factor as a free parameter, it is obvious the fit does not describe the centered peak. We will get back to this problem later.

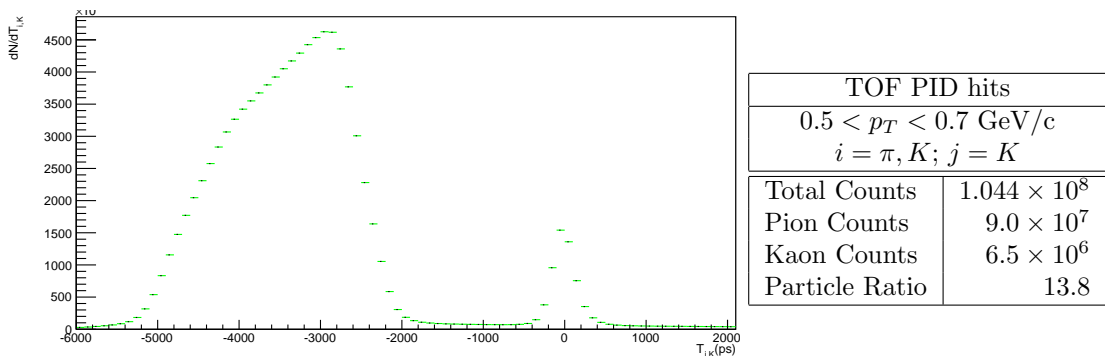
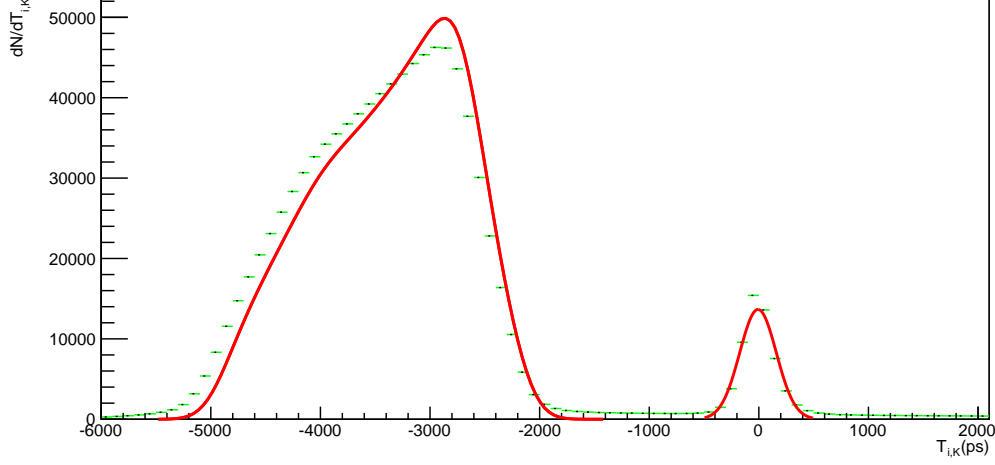
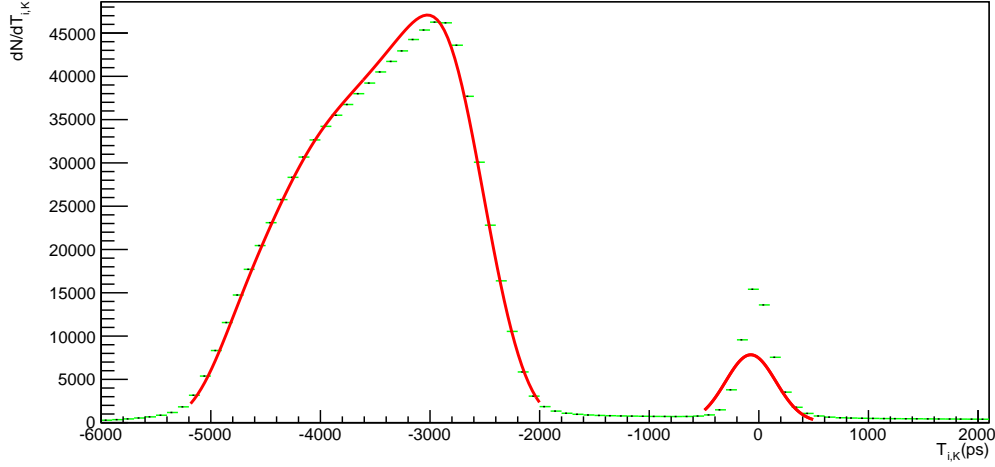


Figure 13: TOF PID hits in Pb-Pb collisions of pions and kaons ($i = \pi$ and $i = K$) with a kaon expectation ($j = K$) for $0.5 < p_T < 0.7$ GeV/c. Total number of hits: 1.04423×10^8



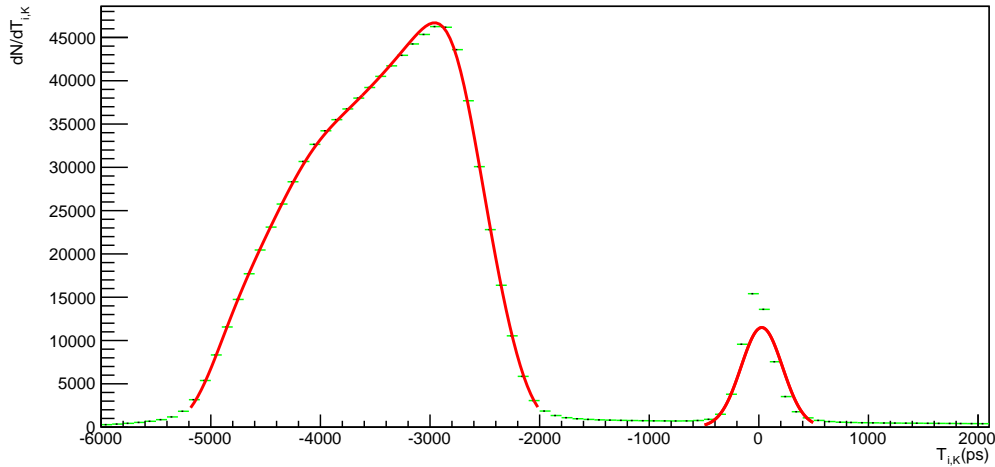
(a) Fit to centered kaon peak (right peak)

TOF PID hits	
$0.5 < p_T < 0.7 \text{ GeV}/c$	
$i = \pi, K; j = K$	
Kaon Fit Parameters	
σ	164 ps
N_K	5.7×10^6
L_{TOF}	3.8m (fixed)
$\chi_{red,K}^2$	9.1×10^6
N_π	8.6×10^7
N_K/N_π	14.9



(b) Fit to deformed pion peak (left peak)

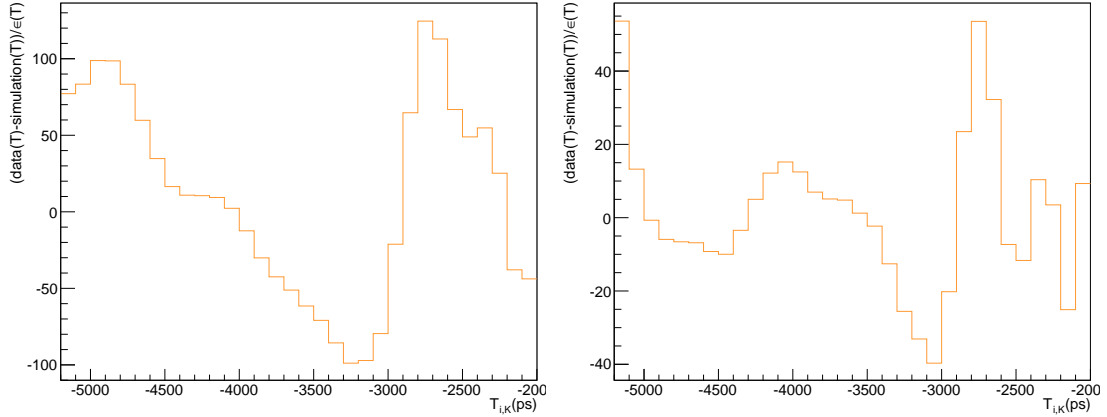
TOF PID hits	
$0.5 < p_T < 0.7 \text{ GeV}/c$	
$i = \pi, K; j = K$	
Pion Fit Parameters	
σ	237 ps
μ	-78 ps
C_0	1
C_1	-0.54
N_π	9.2×10^7
L_{TOF}	3.8m (fixed)
χ_{red}^2	4333



(c) Fit to deformed pion peak (left peak)

TOF PID hits	
$0.5 < p_T < 0.7 \text{ GeV}/c$	
$i = \pi, K; j = K$	
Pion Fit Parameters	
σ	189 ps
μ	27 ps
C_0	1 (fixed)
C_1	-0.64
N_π	8.8×10^7
L_{TOF}	3.9m (fixed)
χ_{red}^2	419

Figure 14: Left peak: The simulated distribution of $dN/dT_{\pi,K}$ (red) plotted against the pion peak of the data (green). Right peak: The Gaussian distribution (red) used for the convolution in the simulation plotted against the centered kaon peak (green) of the data. Total number of hits: 1.04423×10^8



(a) “Normalized Residual” of the fit of Figure 14(b), $\chi_{red}^2 = 4333$, (b) “Normalized Residual” of the fit of Figure 14(c), $\chi_{red}^2 = 419$

Figure 15: “Normalized Residual” – difference between the yield and the simulation divided by the error of the yield $\epsilon = \sqrt{N}$.

The first fit in Figure 14(a) has its pion peak shifted to smaller T_{ij} with respect to the data. Also, the simulation is too narrow in (a) and to a lesser extent also in (b). In (b) this is reflected in the negative value for μ and the large standard deviation of $\sigma = 237$ ps that has to make up for the width of the simulation. Increasing the length of the radius of the TOF detector will shift our simulation to larger T_{ij} and also ‘stretch’ up the width of the peak. Although we know the radius of 3.8m to be correct within a few centimeters, adjusting the radius will help us explore what would improve our simulation. Figure 14(c) shows the result of a fit with a radius of $L_{TOF} = 3.9$ m. This fit has a Chi-squared of $\chi_{red}^2 = 419$. Though the Chi-squared is still much bigger than 1, it is the best fit so far and a significantly better fit is not possible with these parameters.

5.3 Fit to deformed peak with exponential tail and constant added

The PID TOF resolution is better fitted by a Gaussian function with a decreasing exponential tail added on the right side of the peak. It is unknown what causes the shape if this distribution. An example of a typical PID TOF resolution is shown in Figure 16. For a $p > 0$ this function can be expressed as:

$$f(x) = \begin{cases} G(x) = \frac{1}{\sigma\sqrt{2\pi}} \exp\left(\frac{-(x-\mu)}{2\sigma^2}\right) & \text{for } T_{ij} < p \\ E(x) = E_0 \exp\left(\frac{-x}{E_1}\right) & \text{for } T_{ij} > p \end{cases} \quad (19)$$

With the constraints that $G(p) = E(p)$ and $G'(p) = E'(p)$ to make the function continuous. The

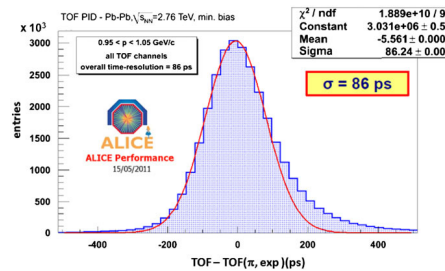


Figure 16: TOF PID resolution for selected pions [1]

constraints determine the values for E_0 and E_1 :

$$E_1 \equiv \frac{-\sigma^2}{(\mu - p)} \quad (20)$$

$$E_0 \equiv \frac{1}{\sigma\sqrt{2\pi}} * \exp\left(\frac{p}{E_1} - \frac{(p - \mu)^2}{2 * \sigma^2}\right) \quad (21)$$

This leaves us with one extra parameters to fit: p .

Another parameter can be added to improve the fit. The big χ_{red}^2 for the fit on the kaon peak in Figure 14(a) is largely due to the background noise we see on both sides of the peak. We simulate this noise by adding a constant B_0 to the function:

$$f(x) = \begin{cases} G(x) = \frac{1}{\sigma\sqrt{2\pi}} \exp\left(\frac{-(x-\mu)}{2\sigma^2}\right) + B_0 & \text{for } T_{ij} < p \\ E(x) = E_0 \exp\left(\frac{-x}{E_1}\right) + B_0 & \text{for } T_{ij} > p \end{cases} \quad (22)$$

Figure 18(a) shows the result of the fit including the exponential tail and the added constant as parameters. We now are able to fit a wider range, but still not very successful since we have a that $\chi_{red}^2 = 1813$. Note that this χ_{red}^2 is an improvement on our last fit with $L_{TOF} = 3.8\text{m}$ in Figure 14(a).

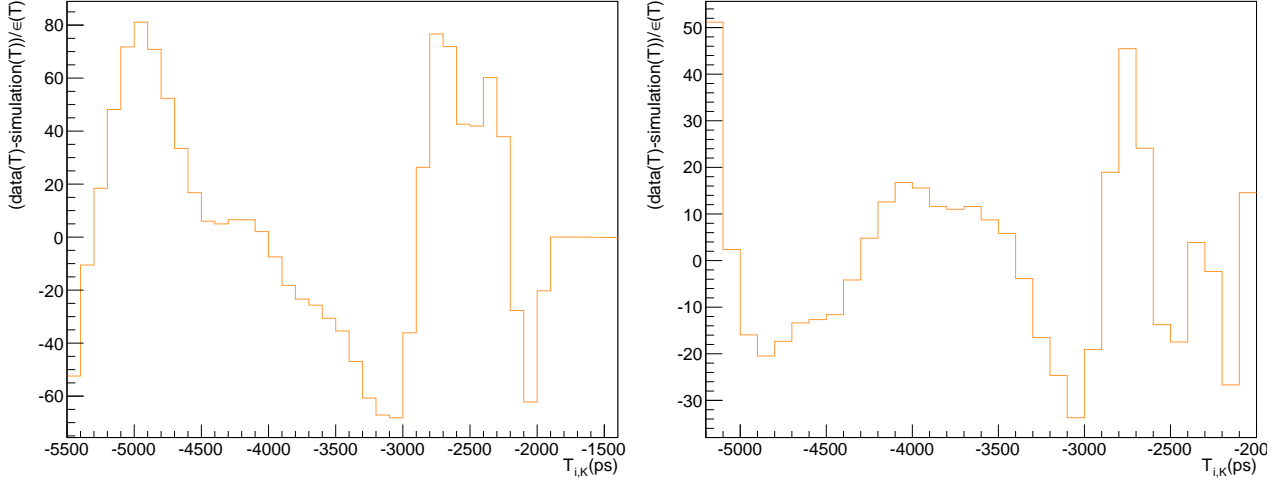
5.4 Fit to deformed peak with scaling factor

The fact that the simulation fitted best when we changed the L_{TOF} from 3.8m to 3.9m tells us the problems with our fits have something to do with a scaling factor. The radius of the TOF varies between 3.75m and 3.86m, so there is no good reason to use an L_{TOF} of 3.8m in our fit. Therefore we are looking for a way to scale without having to adjust L_{TOF} . We scale our Splines by using $S(\frac{T}{scale})$, stretching up the shape of the Splines. Admittedly this is a crude method, but for now it will suffice as a tool to explore how future improvements on our model could be made. We let go of the expression for the resolution in Equation (22) and convolute a Gauss with the scaled Splines. Figure 18(b) shows the resulting fit. Although this is the best fit with a $\chi_{red}^2 = 379$, the simulation still does not fit the kaon peak ($\chi_{red}^2 = 81, 268$).

One of the problems of all our fits is that we cannot seem to use the same parameters for both peaks. We started out assuming them to be the same since they are both subject to the same TOF resolution, this assumption apparently cannot be made and the resolutions must be different for each particle.

All fits are consistent in giving us negative values for C_1 within an average of -0.62 . This means all fits indicate a negative slope in the momentum spectrum at the momentum range $0.5 < p_T < 0.7 \text{ GeV}/c$. This is consistent with the negative slopen in Figure 3 although the slope seems to differ by a factor of ten.

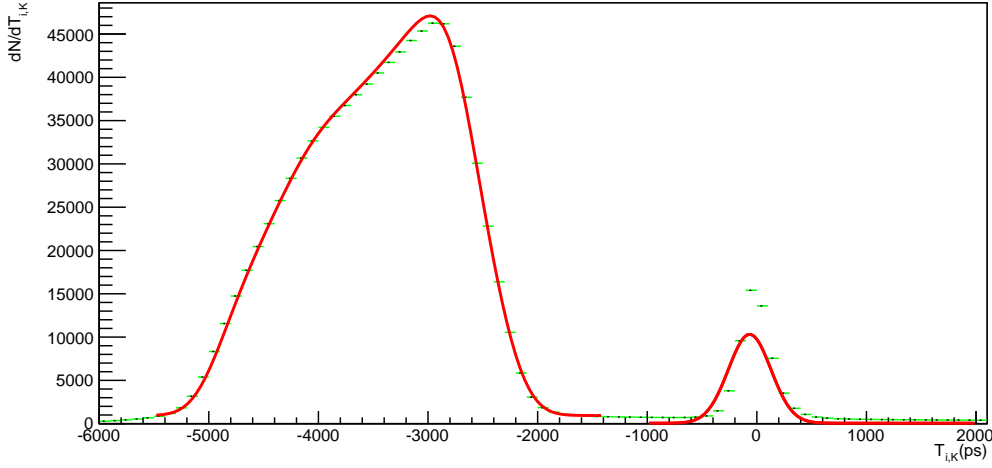
Throughout all fits the σ is bigger than we expect. Although the resolution does vary for the momentum, the large σ 's are probably an effect of the bad fit. A large σ smoothens out the simulation compensating for deviations.



(a) “Pull” of the fit of Figure 18(a), $\chi_{red}^2 = 2216$

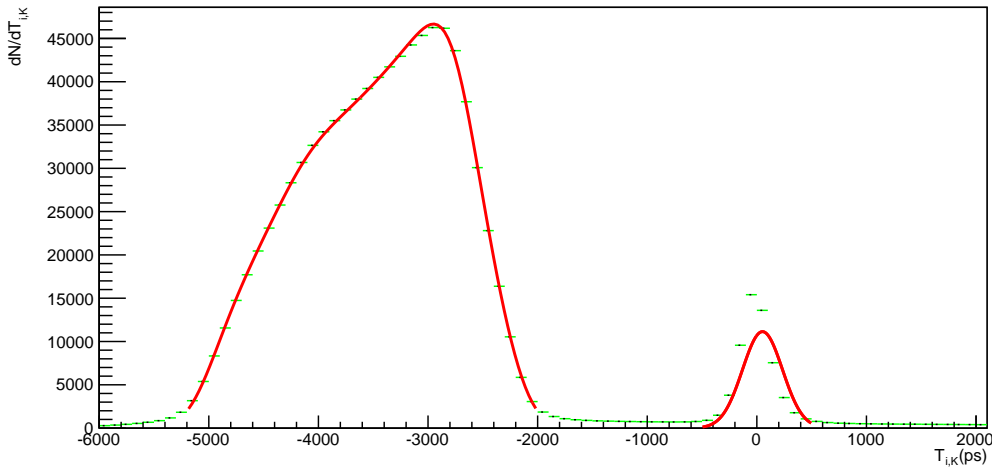
(b) “Pull” of the fit of Figure 18(b), $\chi_{red}^2 = 379$

Figure 17: “Pull” – difference between the yield and the simulation divided by the error of the yield $\epsilon = \sqrt{N}$.



(a) Fit to pion peak (left peak)

TOF PID hits	
$0.5 < p_T < 0.7 \text{ GeV}/c$	
$i = \pi, K; j = K$	
Pion Fit Parameters	
σ	194 ps
μ	-66 ps
C_0	1
C_1	-0.63
p	500 ps
B_0	1.09×10^{-5}
L_{TOF}	3.8m (fixed)
χ_{red}^2	1813



(b) Fit to pion peak (left peak)

TOF PID hits	
$0.5 < p_T < 0.7 \text{ GeV}/c$	
$i = \pi, K; j = K$	
Pion Fit Parameters	
σ	182 ps
μ	52 ps
C_0	1
C_1	-0.63
scaling	1.037
N_π	8.5×10^7
L_{TOF}	3.8m (fixed)
$\chi_{red,\pi}^2$	379
$\chi_{red,K}^2$	81,268
N_K	5.09×10^6
N_K/N_π	16.7

Figure 18: Left peak: The simulated distribution of $dN/dT_{\pi,K}$ (red) plotted against the pion peak of the data (green). Right peak: The Gaussian distribution (red) used for the convolution in the simulation plotted against the centered kaon peak (green) of the data. Total number of hits: 1.04423×10^8 .

6 Conclusion and Outlook

It was shown that the deformed peak shapes in a TOF PID histogram can be simulated. First with a Monte Carlo method, generating virtual particles and determining their time of flight. Secondly, with a numerical Spline function that entailed a coordinate transformation of the momentum and pseudorapidity distributions. The Monte Carlo simulation and Numerical Spline function are consistent with each other, which gives us confidence the processing of equations in the simulations was successful. Fitting the our numeric Spline to the data was less successful. This model might be a good start, when first glancing at it the reproduced peak shapes seem to resemble the data very much. But the $\chi_{red}^2 = 4333$ of a straight forward fit indicates improvements should be made. A better $\chi_{red}^2 = 419$ was found changing the radius of the detector by 10cm. And the best fit with $\chi_{red}^2 = 379$ integrated a scaling factor of which the origin is unknown. These adjustments were crude and only justified within the scope of further research. The consistency in the unconvoluted dN/dT distributions of the different simulation methods leads to the conclusion that improvements should be sought after in the convolution. For instance, in the simulation we used a constant value for σ , however σ is dependent of the momentum. Integrating a variable σ into the simulation might be worth investigating.

7 Acknowledgments

I would like to thank Misha Veldhoen for answering all my questions during a very helpful and friendly supervision. I would like to thank Marco van Leeuwen for his advising role and patience.

References

- [1] A. Alici, Nucl. Instr. Meth. A 706 29-32 (2013), *The MRPC-based ALICE time-of-flight detector: Status and performance*
- [2] ALICE Collaboration, R. Preghenella, arXiv:1203.5904 [hep-ex] (2013), *Spectra of identified hadrons with the ALICE detector in pp and Pb-Pb collisions at the LHC*
- [3] <http://aliceinfo.cern.ch/>